NANO LETTERS

Letter

pubs.acs.org/NanoLett

Bond Elasticity Controls Molecular Recognition Specificity in Antibody−Antigen Binding

Anna Alemany,[†] Nuria Sanvicens,[‡] Sara de Lorenzo,[†] M.-Pilar Marco,[‡,§] and Felix Ritort*[,†,§]

[†]Small Biosystems Lab, Department Física Fonamental, Universitat de Barcelona, C/Martí i Franquès 1, 08028 Barcelona, Spain

[‡]Nanobiotechnology for Diagnostics (Nb4D) group, Centro Superior de Investigaciones Científicas, C/Jordi Girona 18-26, 08034 Barcelona, Spain

[§]Networking Research Center of Bioengineering, Biomaterials and Nanomedicine (CIBER-BBN), Instituto Carlos III, C/Sinesio Delgado 4, 28029 Madrid, Spain

Supporting Information

ABSTRACT: Force-spectroscopy experiments make it possible to characterize single ligand−receptor pairs. Here we measure the spectrum of bond strengths and flexibilities in antibody−antigen interactions using optical tweezers. We characterize the mechanical evolution of polyclonal antibodies generated under infection and the ability of a monoclonal antibody to cross-react against different antigens. Our results suggest that bond flexibility plays a major role in remodeling antibody−antigen bonds in order to improve recognition during the maturation of the humoral immune system.

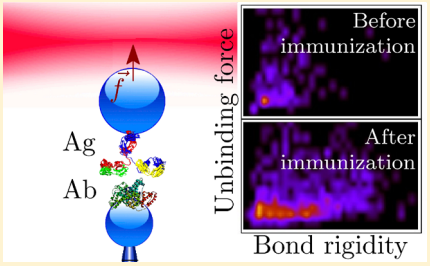

KEYWORDS: *Antibody−antigen recognition, optical tweezers, bond specificity, bond flexibility, single-molecule methods*

Intermolecular recognition is an ubiquitous phenomenon in biological systems, like cellular adhesion, cell signaling, or the regulation of replication and transcription of nucleic acids. Noteworthy, molecular recognition is crucial in the humoral immune system of vertebrate organisms, where antibodies can specifically identify a single foreign body (antigen) among thousands of molecules.

A proper understanding of the mechanisms that govern the immune response is critical to the optimal performance of antibody-based therapies and techniques. Therefore, the investigation of molecular interactions and the characterization of antigen-binding affinity constitutes a major area of interest. Traditional studies[1−4] use nuclear magnetic resonance spectroscopy, crystallographic analysis, surface plasmon resonance, or fluorescence microscopy to characterize biophysical properties of bonds such as affinity, dissociation rate constants, or epitope binding sites.

Several studies have indirectly shown that specificity and rigidity are related properties of intermolecular bonds.[5−8] Recently, Romesberg and collaborators[9−11] used photon echo spectroscopy and related the time scales of intermolecular bond motion to the degree of flexibility of the interaction, which provided a novel method to characterize bond elasticity as a function of bond affinity. Experimental evidence suggests that bond elasticity is a key feature controlling the response of the immune system to infection: at the initial stages, the detection of intrusive agents is mainly nonspecific; antibodies are very elastic and continuously explore different conformations, which enables them to bind as many antigens as possible. Resulting intermolecular bonds are expected to be very flexible and varied, and despite being suboptimal interactions they may reorganize their structure to increase binding strength.[12] After the detection, a complex immunitary response entailing the massive production of different antibodies takes place.[13,14] This process, known as the maturation line of the immune system, triggers the appearance of new antibodies that specifically bind to destroy a given foreign body through rigid bonds. Interestingly, such new antibodies do not lose their ability to explore multiple conformations and cross-react with different antigens, which promotes the recognition of newer infections through the establishment of elastic nonspecific bonds. Therefore, direct measurements of the elastic properties of ligand−receptor bonds can be crucial to understand the relation between bond affinity and bond rigidity.

In the past decade, advances in the mechanical manipulation of receptor−ligand bonds at the level of individual molecular pairs have been possible thanks to the improvement of experimental techniques such as atomic force microscopy, biomembrane force probe transducer, and laser optical tweezers.[15−17] Optical tweezers are ideally suited to characterize the elastic response of polymers to applied mechanical forces.[18−20] Moreover, they are an emergent tool to investigate the effect of force on single antibody−antigen interactions because of their accessible force-range (0−80 pN) and resolution (∼0.1 pN).[21−30] In this work, for the first time we use optical tweezers to characterize the correlation between bond flexibility and mechanical strength.

Received: July 16, 2013
Revised: September 17, 2013
Published: September 27, 2013

dx.doi.org/10.1021/nl402617f | *Nano Lett.* 2013, 13, 5197−5202

We have first investigated the relation between the decrease in flexibility with the increase in specificity in intermolecular bonds using a polyclonal system obtained before and after immunization. To this end, a rabbit was inoculated with a complex made by methyl-boldenone (MB) linked to the carrier protein horseshoe crab hemocyanin (HCH).[31] Polyclonal antibodies present in the animal blood before immunization (hereafter referred as preimmunological antibodies, PreI) and after immunization (Pab) were isolated.[32] Then, a 3 μm-diameter polystyrene bead coated with antibodies (PreI or Pab) was captured in the optical trap (see Supporting Information S1 and S2). A second 2 μm-diameter polystyrene bead coated with MB linked to bovine serum albumin (BSA) (to focus the attention of antibodies that specifically recognize MB, HCH was replaced by BSA here) was kept fixed in the tip of a micropipet by air-suction (Figure 1a). The coupling efficiency

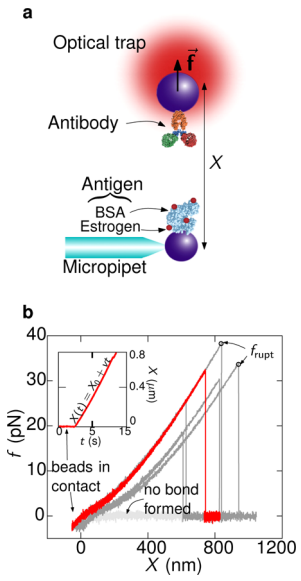

Figure 1. Force-spectroscopy experiments. (a) Experimental scheme (figure not to scale). One bead coated with antibodies is captured in the optical trap. Another bead coated with antigens is immobilized in the tip of a micropipet by air suction. The beads are approached by varying the trap-pipet distance X. (b) Pulling experiments. Inset: beads are kept in mutual contact at −3 pN for 2 s. Next X is increased at a constant speed v, around 140 nm/s if not stated otherwise. Main panel: different examples of force−distance curves. After contact, the force remains zero in the absence of a binding event (light-gray curve). When a bond is successfully established the force increases until the value f_{rupt} is reached and then it drops to zero (red and dark-gray curves). A minimum of 5 and a maximum of 70 pairs of beads were tested for each interaction under study and at least 80 pulling curves per pair of beads were recorded.

of the immunoreagents to the polystyrene beads was checked (see Supporting Information S1) and the result was similar in all cases. At the beginning of a pulling experiment (Figure 1b), the two beads are kept at a contact force of −3 pN for 2 s, enabling the molecules on the surface to interact. Next, the distance between the center of the optical trap and the tip of the micropipet, X, is increased at a constant pulling speed v (Figure 1b, inset). After contact, either no interaction is established and the force remains zero (light-gray curve in Figure 1b) or a bond is formed (red and dark-gray curves) and the force increases until the bond breaks at the so-called rupture force, f_{rupt}, and the force drops to zero. Some traces (less than 10%) show two or more rupture forces, indicating multiple binding, that is, the formation of parallel bonds. To focus our attention on single bonds such events are not taken into account. However, sometimes multiple bonds can break at the same time and cannot be discriminated within our limited time-resolution measurement (a few milliseconds). To remove these simultaneous multiple unbinding events we use a statistical method previously introduced by Evans and collaborators[22] (see Supporting Information S3).

We observe large variability in the slopes of different force−distance curves (Figure 1b), which suggests a diversity of antibody−antigen bonds. Two sources may contribute to such variability. First, the heterogeneous population of antibodies present in the PreI and Pab samples. Second, the diversity of conformational substates for each antibody that are functional and bind to the antigen.[5,6,33] In order to evaluate the degree of affinity of each set of antibodies to MB, control experiments between Pab-/PreI-coated beads and BSA-coated beads were also carried out.

In Figure 2a, we show the binding efficiencies of pulling experiments, defined as the ratio between the number of

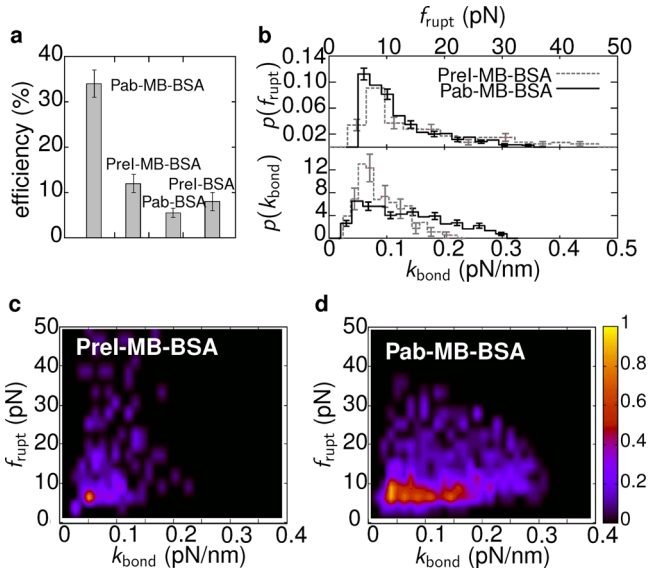

Figure 2. Maturation line for MB. (a) Binding efficiencies in pulling experiments with polyclonal antibodies PreI and Pab tested against the complex MB-BSA (error bars are standard errors over different tested pairs of beads). (b) Histograms of f_{rupt} (top) and k_{bond} evaluated at 5 pN (bottom) measured with polyclonal antibodies PreI (dashed line) and Pab (solid line) tested against the complex MB-BSA. Error bars are the standard deviation and were obtained using the Bootstrap method. The 2D contour plot with histograms of f_{rupt} plotted against histograms of k_{bond} measured in pulling experiments using the complex MB-BSA and PreI (c) or Pab (d).

successful binding events to the total number of times the pair of beads were put in mutual contact, for the different samples. In order to discriminate rupture events from thermally induced force fluctuations, rupture force events below 3 pN were discarded. The binding efficiency between Pab and the complex MB-BSA is almost 35%, whereas between Pab and BSA is lower than 15%. This proves that the immune system develops antibodies that accurately detect MB, even if the immunization has been performed by linking them to a big carrier protein such as HCH. On the other hand, the binding efficiencies measured between PreI and MB-BSA or BSA (10−15%) are

dx.doi.org/10.1021/nl402617f | Nano Lett. 2013, 13, 5197−5202

comparable. This indicates that both PreI and Pab detect BSA with an almost identical low affinity, which suggests nonspecific recognition.

The histograms of f_{rupt} for successful binding events for PreI-MB-BSA and Pab-MB-BSA are very similar (Figure 2b top). In contrast, the histogram of bond rigidities measured at 5 pN (k_{bond}, see Supporting Information S4) for the Pab-MB-BSA case extends to higher values as compared to the one obtained for the PreI-MB-BSA case (Figure 2b bottom). In order to gain more information about differences between the preimmunological and specific polyclonal recognition to MB we study the correlation between bond elasticity and rupture forces. We use 2D contour plots with histograms of f_{rupt} plotted against histograms of k_{bond},[34] which reveal direct correlation between specific recognition and bond elasticity. Figure 2c,d shows such plots for the recognition events measured in pulling experiments testing PreI and Pab against MB-BSA, respectively. In the case of PreI, we observe that most binding events have f_{rupt} below 10 pN and k_{bond} below 0.1 pN/nm (Figure 2c, purple-orange-yellow region). Moreover, the purple scattered regions in Figure 2c show that some PreI-MB-BSA bonds, despite being nonspecific, are able to structurally reorganize in order to increase binding strength, which implies an increase in f_{rupt}. In the case of Pab, successful binding events cover a wider interval of rupture forces and new regions in the 2D contour plot are populated at high values of k_{bond} (from 0.1 to 0.3 pN/nm, Figure 2d). This indicates that interactions measured between PreI and MB-BSA are weaker and more flexible than the ones measured using Pab and the same antigen. Therefore, we observe that the immune system has generated new antibodies that recognize MB through more rigid bonds.

A similar procedure can be applied to study the cross-reactivity of antibodies. In this case, a monoclonal antibody (Mab) was produced against the anabolic steroid boldenone (B).[32] It is expected that this antibody also has affinity for testosterone (T), which is another steroid hormone that shares the rings *B*, *C*, and *D* in common with B (Figure 3a). Pulling experiments were carried out to prove the ability of Mab to cross-react against the two similar haptens and to quantify its different binding strengths to different antigens. As in the case of MB, both B and T were linked to BSA.

In Figure 3b, we show the experimental binding efficiencies obtained between Mab and B-BSA, T-BSA or BSA. As expected, the highest value is found for Mab tested against the complex B-BSA, followed by the one measured between Mab tested against T-BSA. Finally, the efficiency reported for the recognition between Mab and BSA is the lowest.

The histograms of f_{rupt} (Figure 3c top) for the three bonds Mab-B-BSA (solid line), Mab-T-BSA (dashed line) and Mab-BSA (dotted line) show different features from each other. In the Mab-B-BSA case, a maximum in rupture forces around 30 pN is revealed, whereas in the Mab-T-BSA case a shoulder can be seen around 20 pN with positive deviation with respect to the Mab-BSA case. Both behaviors suggest recognition from Mab to B and T with different degrees of affinity. The histograms of k_{bond} (Figure 3c bottom) are also evaluated and a maximum around 0.1 pN/nm is obtained for the three cases. However, $p(k_{bond})$ for Mab-B-BSA shows a lower deviation with respect to the other cases at larger values of k_{bond}.

Again, the 2D contour plot of histograms of f_{rupt} and k_{bond} reveal features of the different antibody−antigen bonds that get masked with the conventional histograms $p(k_{bond})$ and $p(f_{bond})$. In Figure 3d the case for recognition between Mab and BSA is

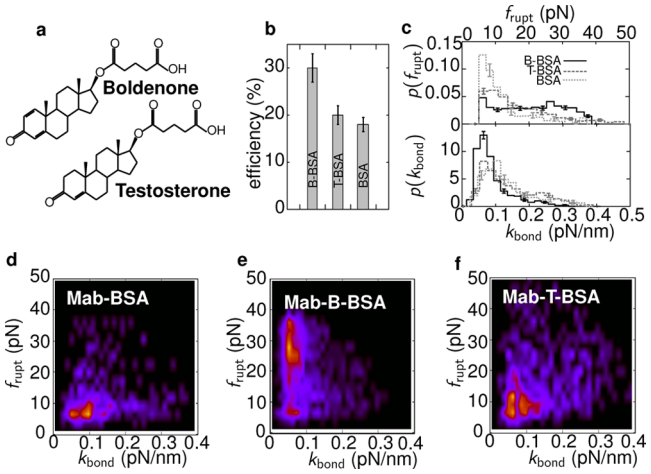

Figure 3. Cross-reactivity of a monoclonal antibody. (a) Chemical structures for the haptens of boldenone (B) and testosterone (T) used in force-spectroscopy experiments. (b) Binding efficiencies in pulling experiments using Mab against different antigens (error bars are standard errors over different tested pairs of beads). (c) Histograms of f_{rupt} (top) and k_{bond} evaluated at 5 pN (bottom) measured with Mab tested against B-BSA (solid line), T-BSA (dashed line) and BSA (dotted line). Error bars are the standard deviation, and were obtained using the Bootstrap method. The 2D contour plots with histograms of f_{rupt} plotted against histograms of k_{bond} measured in pulling experiments using Mab and BSA (d), B-BSA (e), and T-BSA (f).

shown. A broad range of bond elasticities at low values of rupture forces is covered (purple-orange-yellow region). This suggests that the bond Mab-BSA is able to explore several structural conformations with different degrees of flexibility in order to increase its binding affinity. Such a result combined with the observed low efficiency in pulling experiments (<20%, Figure 3b) indicates that the interaction between Mab and BSA is mainly nonspecific, in agreement with results obtained with polyclonal antibodies (Figure 2). An extremely different pattern is obtained for the recognition between Mab and B-BSA (Figure 3e): at forces below 10 pN the 2D contour plot is very similar to the one measured for the Mab-BSA bond (Figure 3d), which indicates that in this region interactions between Mab and BSA mainly occur. Remarkably the Mab-B-BSA bond also covers values of f_{rupt} ranging from 20 to 40 pN (orange-yellow area). Such region is not populated by the Mab-BSA bond. This is a signature of specific recognition between Mab and B.

In the 2D contour plot of histograms of f_{rupt} and k_{bond} for Mab-T-BSA (Figure 3f), we observed that most rupture forces are found below 30 pN and a wide interval of bond rigidities is covered (k_{bond} ~0.05−0.3 pN/nm). Such results reveal that Mab recognizes T and it is able to establish stronger bonds with T than with BSA. However, the large range of rigidities covered suggests that the bond explores different conformations in order to improve recognition. Hence, Mab shows cross-reactivity, being able to recognize antigens that are similar to B (such as T) but with different degrees of affinity, as revealed by the different correlation patterns of f_{rupt} and k_{bond}.

The scattered purple regions observed in Figure 3d−f suggest diversity of antibody−antigen bonds. It has been hypothesized that such diversity is the seed of improved recognition specificity by antibodies.[3,6,7,12] Accordingly, non-specific antibody−antigen bonds explore multiple conformations in order to improve specificity and therefore they must

dx.doi.org/10.1021/nl402617f | *Nano Lett.* 2013, 13, 5197−5202

have low activation barriers and multiple binding states. In contrast, activation barriers for specific bonds must be large to guarantee an optimized response to the infection.[35,36]

In order to characterize the main features of the free-energy landscape (FEL) of specific Mab-B and Mab-T bonds we first need to remove nonspecific events where Mab most probably recognized BSA instead of B or T. Several one-dimensional approaches, based only on rupture forces, have been previously suggested in literature.[15,30] Here, we use a two-dimensional Bayesian inference approach that takes into account correlations between k_{bond} and f_{rupt} (see Supporting Information S5 for details). Figure 4a,b shows the resulting 2D contour plots of the histograms of f_{rupt} against k_{bond} for Mab-B and Mab-T.

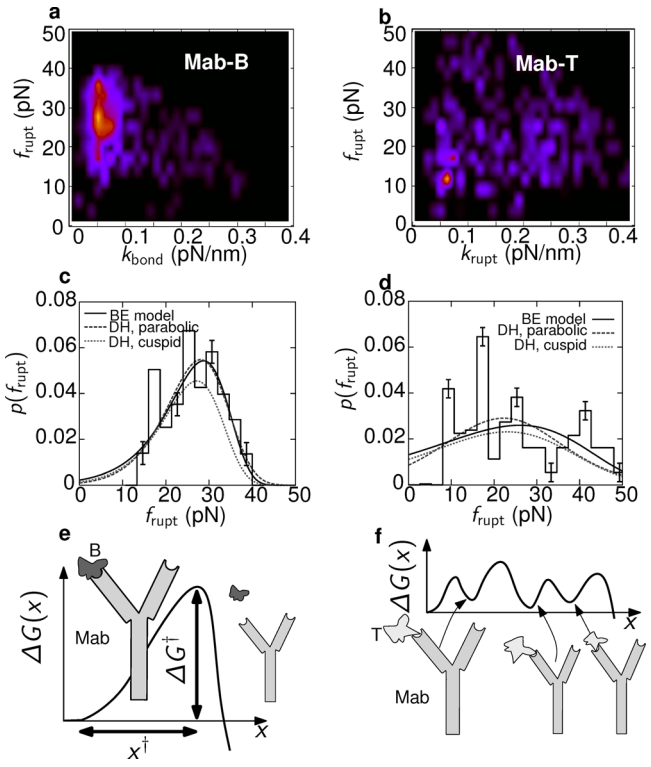

Figure 4. Free-energy landscape of the specific bonds Mab-B and Mab-T. The 2D contour plot of the specific recognition between Mab and B (a) and between Mab and T (a) (see also Supporting Information Figures S1 and S2). Experimental rupture force histogram and fits to the BE model (continuous line), the DH model with a parabolic FEL (dashed) or a cubic FEL (dotted) for the bond Mab-B (c) and the bond Mab-T (d). (e) Sketch of the FEL of the Mab-B bond with a single escape barrier and a single bond state. (f) Sketch of the FEL of the Mab-T bond with multiple states and low kinetic barriers are low.

Most well-accepted models of the force-induced breakage of molecular bonds are the Bell-Evans (BE)[15,37] and the Dudko-Hummer (DH)[38] models. Both cases consider a FEL with a single escape barrier and provide analytical expressions for the probability density function of rupture forces in pulling experiments $p(f_{rupt})$ (see Supporting Information S6), which we measured by projecting the specific 2D contour plots into the force axis. Figure 4c,d shows the fits of the BE and DH models to experimental data from which we obtain estimations of the attempt rate of dissociation at zero force, k_0; the distance between the bonded and the transition state, $x^{\dagger}$; and the height of the kinetic barrier, $\Delta G^{\dagger}$. Results are given in Table 1, and compatibility between different fits is found within error bars.

Values obtained using different procedures for $x^{\dagger}$ for both Mab-B and Mab-T bonds are in agreement between themselves and with those reported in previous single-molecule studies carried out on different antibody−antigen systems.[22,30] For any fit, the estimated value of k_0 for the Mab-T bond is almost ten times larger than the one estimated for the Mab-B bond (Table 1), indicating a larger bond lifetime at zero force (i.e., k_0^{-1}) for the latter. Moreover, a larger kinetic barrier $\Delta G^{\dagger} \sim 17\ k_BT$ is found for the bond Mab-B as compared to the one reported for Mab-T, $\Delta G^{\dagger} \sim 3\ k_BT$. Finally, we observe that the rupture force histogram for the specific bond Mab-T is not accurately fitted for any model (Figure 4d). All these facts suggest that the specific recognition between Mab and B has a large affinity and can be modeled with a FEL made of a bonded state and a single escape barrier (Figure 4e). In contrast, for the Mab-T bond the affinity is lower and a single escape barrier does not fit the rupture force histogram. In this case, the recognition is less specific, and its FEL should be more appropriately described by several states and lower kinetic barriers[36,39] (Figure 4f).

Taking into account that the FEL of the Mab-B bond can be described with a single escape barrier we performed pulling experiments at different pulling speeds. Results are summarized in the Supporting Information Section S7, and are in good agreement within error bars with estimations summarized in Table 1.

In summary, in this work we have applied force-spectroscopy techniques to study the specificity of binding between antigens and antibodies by measuring the spectrum of bond elasticities and mechanical strengths in single-bond pulling experiments using optical tweezers. This novel approach has been used to unravel different binding mechanisms used by polyclonal and monoclonal antibodies tested against different antigens. We have seen that in order to improve the specificity in the antibody−antigen recognition, antibodies generated after immunization establish stronger bonds with lower flexibilities than antibodies prior to immunization (Figure 2). Consequently, we show that bonds strengthen and become more rigid as ligand−receptor affinity increases. Our results on the

Table 1. Results from Fits of Specific Rupture Force Histograms $p(f_{rupt})$ (Fig. 4c, d) to the BE and the DH Models[a]

	Mab-B			Mab-T		
FEL model	$x^{\dagger}$ (Å)	k_0 (s^{-1})	$\Delta G^{\dagger}$ (k_BT)	$x^{\dagger}$ (Å)	k_0 (s^{-1})	$\Delta G^{\dagger}$ (k_BT)
BE	6.0 ± 1.0	0.008 ± 0.003		2.5 ± 1.0	0.05 ± 0.01	
DH, parabolic	9.5 ± 1.0	0.003 ± 0.001	12 ± 4	5.0 ± 1.0	0.03 ± 0.01	4.0 ± 1.0
DH, cubic	8.0 ± 1.0	0.005 ± 0.002	14 ± 5	3.0 ± 1.0	0.04 ± 0.01	4.0 ± 1.0

[a]In the BE model, $k_0 = \omega_0 \exp[(-\Delta G^{\dagger})/(k_BT)]$ (Supporting Information Information S5.1). Therefore, to estimate $\Delta G^{\dagger}$ we need to assume a value for ω_0. For instance, if we take[40,41] $\omega_0 \sim 10^5$−10^7 s^{-1} we get $\Delta G^{\dagger} \sim 17$−$21\ k_BT$ for Mab-B and $\Delta G^{\dagger} \sim 15$−$19\ k_BT$ for T. Error bars are standard errors from fit.

dx.doi.org/10.1021/nl402617f | Nano Lett. 2013, 13, 5197−5202

cross-reactivity of monoclonal antibodies also suggest that nonspecific antibody−antigen interactions explore different conformations to increase bond-specificity and improve molecular recognition. This is revealed by the broad spectrum of rigidities that can be measured in pulling experiments for different nonspecific interactions (Figures 2c and 3d). Such diversity might be due both to an heterogeneous population of polyclonal antibodies present in the sample and to a diversity of conformational substates for each monoclonal antibody that are functional and bind to the antigen. This behavior is in agreement with previous studies,[5,6,8,33,42,43] where the nonspecific antibody−antigen bond is modeled by combining the conformational-change and the induced-fit mechanisms of binding. In the first case, antigens and antibodies explore different conformations before binding and transient molecular states interact when structures match each other. In the second case, initial unoptimized bonds explore the conformational space and reorganize their structure in order to increase the binding strength. Such multiplicity of conformational states or kinetic barriers is not surprising. Seminal investigations have already shown functionality of multiple conformational states characterized by different activation barriers.[44,45] These results suggest a crucial role of bond heterogeneity in the humoral immune system. Overall, they reinforce the intriguing possibility of understanding the immune system in terms of evolutionary allosteric macromolecular ensembles governed by the flexural property of antibody−antigen bonds.

Future studies should address the detailed continuous adaptation in time of the humoral immune system to a given infection by characterizing the full time-evolution of the degree of flexibility of antibody−antigen bonds. Ultimately, the mechanistic approach might be suitable to unravel and characterize different binding mechanisms used by the antibody repertory to identify infectious agents.

■ ASSOCIATED CONTENT

Supporting Information

Synthesis details, description of the optical tweezers setup, data-analysis techniques, and summary of theoretical models to study the force-induced breakage of molecular bonds are available. This material is available free of charge via the Internet at http://pubs.acs.org.

■ AUTHOR INFORMATION

Corresponding Author

*E-mail: ritort@ub.edu.

Notes

The authors declare no competing financial interests.

■ ACKNOWLEDGMENTS

A.A. acknowledges financial support from Grant AP2007-00995 (Spanish Research Council) and from a “Lanzadera” Grant (CIBER-BBN, 2007). F.R. is supported by Grants FIS2010-19342 and Icrea Academia 2008. We thank Dr. Marco Ribezzi-Crivellari and Gloria de las Heras for fruitful discussions.

■ REFERENCES

(1) Fields, B. A.; Goldbaum, F. A.; Dall'Acqua, W.; Malchiodi, E. L.; Cauerhff, A.; Schwarz, F. P.; Ysern, X.; Poljak, R. J.; Mariuzza, R. A. *Biochemistry* **1996**, *35*, 15494−15503.
(2) Homola, J. *Anal. Bioanal. Chem.* **2003**, *377*, 528−539.
(3) Rosen, O.; Anglister, J. *Methods Mol. Biol.* **2009**, *524*, 37−57.
(4) Liu, W.; Meckel, T.; Tolar, P.; Sohn, H. W.; Pierce, S. K. *J. Exp. Med.* **2010**, *207*, 1095−1111.
(5) Berger, C.; Weber-Bornhauser, S.; Eggenberger, J.; Hanes, J.; Plückthun, A.; Bosshard, H. R. *FEBS Lett.* **1999**, *450*, 149−153.
(6) Ma, B.; Shatsky, M.; Wolfson, H. J.; Nussinov, R. *Protein Sci.* **2002**, *11*, 184−197.
(7) Manivel, V.; Sahoo, N. C.; Salunke, D. M.; Rao, K. V. *Immunity* **2000**, *13*, 611−620.
(8) Sundberg, E. J.; Mariuzza, R. A. *Adv. Protein Chem.* **2002**, *61*, 119−160.
(9) Jimenez, R.; Salazar, G.; Baldridge, K. K.; Romesberg, F. E. *Proc. Natl. Acad. Sci. U.S.A.* **2003**, *100*, 92−97.
(10) Jimenez, R.; Salazar, G.; Yin, J.; Joo, T.; Romesberg, F. E. *Proc. Natl. Acad. Sci. U.S.A.* **2004**, *101*, 3803−3808.
(11) Thorpe, I. F.; Brooks, C. L. *Proc. Natl. Acad. Sci. U.S.A.* **2007**, *104*, 8821−8826.
(12) Boehr, D. D.; Nussinov, R.; Wright, P. E. *Nat. Chem. Biol.* **2009**, *5*, 789−796.
(13) Grey, H. *Immunology* **1964**, *7*, 82.
(14) Medzhitov, R.; Janeway, C. A. *Science* **2002**, *296*, 298−300.
(15) Evans, E. *Annu. Rev. Biophys. Biomol. Struct.* **2001**, *30*, 105−128.
(16) Hugel, T.; Seitz, M. *Macromol. Rapid Commun.* **2001**, *22*, 989−1016.
(17) Ritort, F. *J. Phys.: Condens. Matter* **2006**, *18*, R531.
(18) Smith, S. B.; Cui, Y.; Bustamante, C. *Science* **1996**, *271*, 795−798.
(19) Tskhovrebova, L.; Trinick, J.; Sleep, J.; Simmons, R. *Nature* **1997**, *387*, 308−312.
(20) Wang, M. D.; Yin, H.; Landick, R.; Gelles, J.; Block, S. M. *Biophys. J.* **1997**, *72*, 1335−1346.
(21) Baumgartner, W.; Hinterdorfer, P.; Schindler, H. *Ultramicroscopy* **2000**, *82*, 85−95.
(22) Evans, E.; Kinoshita, K.; Simon, S.; Leung, A. *Biophys. J.* **2010**, *98*, 1458−1466.
(23) Helmerson, K.; Kishore, R.; Phillips, W. D.; Weetall, H. H. *Clin. Chem.* **1997**, *43*, 379−383.
(24) Kuo, S. C.; Lauffenburger, D. A. *Biophys. J.* **1993**, *65*, 2191−2200.
(25) Simson, D.; Strigl, M.; Hohenadl, M.; Merkel, R. *Phys. Rev. Lett.* **1999**, *83*, 652−655.
(26) Perret, E.; Benoliel, A.-M.; Nassoy, P.; Pierres, A.; Delmas, V.; Thiery, J.-P.; Bongrand, P.; Feracci, H. *EMBO J.* **2002**, *21*, 2537−2546.
(27) Salomo, M.; Keyser, U. F.; Struhalla, M.; Kremer, F. *Eur. Biophys. J.* **2008**, *37*, 927−934.
(28) Stout, A. L. *Biophys. J.* **2001**, *80*, 2976−2986.
(29) Strigl, M.; Simson, D. A.; Kacher, C. M.; Merkel, R. *Langmuir* **1999**, *15*, 7316−7324.
(30) Wagner, C.; Singer, D.; Ueberschär, O.; Stangner, T.; Gutsche, C.; Hoffmann, R.; Kremer, F. *Soft Matter* **2011**, *7*, 4370−4378.
(31) Maquieira, Á.; Brun, E. M.; Garcés-García, M.; Puchades, R. *Anal. Chem.* **2012**, *84*, 9340−9348.
(32) Kramer, K.; Hubauer, A.; Lausterer, R.; Salvador, J.-P.; Marco, M.-P. *Anal. Lett.* **2007**, *40*, 1461−1472.
(33) Koshland, D., Jr *Proc. Natl. Acad. Sci. U.S.A.* **1958**, *44*, 98.
(34) Živković, J.; Mitrović, M.; Janssen, L.; Heus, H. A.; Tadić, B.; Speller, S. *Europhys. Lett.* **2010**, *89*, 68004.
(35) Strunz, T.; Oroszlan, K.; Schumakovitch, I.; Güntherodt, H.-J.; Hegner, M. *Biophys. J.* **2000**, *79*, 1206−1212.
(36) Thielges, M. C.; Zimmermann, J.; Yu, W.; Oda, M.; Romesberg, F. E. *Biochemistry* **2008**, *47*, 7237−7247.
(37) Bell, G. I. *Science* **1978**, *200*, 618−627.
(38) Dudko, O. K.; Hummer, G.; Szabo, A. *Phys. Rev. Lett.* **2006**, *96*, 108101.
(39) Raible, M.; Evstigneev, M.; Bartels, F. W.; Eckel, R.; Nguyen-Duong, M.; Merkel, R.; Ros, R.; Anselmetti, D.; Reimann, P. *Biophys. J.* **2006**, *90*, 3851−3864.
(40) Bizarro, C. V.; Alemany, A.; Ritort, F. *Nucleic Acids Res.* **2012**, *40*, 6922−6935.

(41) Engel, S.; Alemany, A.; Forns, N.; Maass, P.; Ritort, F. *Philos. Mag.* **2011**, *91*, 2049−2065.
(42) Jerne, N. K. *Proc. Natl. Acad. Sci. U.S.A.* **1955**, *41*, 849.
(43) Pauling, L. *Chem. Eng. News* **1946**, *24*, 1375−1377.
(44) Austin, R.; Beeson, K.; Eisenstein, L.; Frauenfelder, H.; Gunsalus, I.; Marshall, V. *Phys. Rev. Lett.* **1974**, *32*, 403−405.
(45) Solomatin, S. V.; Greenfeld, M.; Herschlag, D. *Nat. Struct. Mol. Biol.* **2011**, *18*, 732−734.

dx.doi.org/10.1021/nl402617f | *Nano Lett.* 2013, 13, 5197−5202